Additive layer manufacturing of titanium matrix composites using the direct metal deposition laser process

Sébastien Pouzet, Patrice Peyre, Cyril Gorny, Olivier Castelnau, T Baudin, F Brisset, C Colin, P. Gadaud

Additive layer manufacturing of titanium matrix composites using the direct metal deposition laser process

S. Pouzet [a,*], P. Peyre [a], C. Gorny [a], O. Castelnau [a], T. Baudin [b], F. Brisset [b], C. Colin [c], P. Gadaud [d]

[a] PIMM Laboratory, UMR 8006 CNRS-Arts et Métiers Paristech – CNAM, 75013 Paris, France
[b] ICMMO, Université de Paris-Sud, 91405 Orsay, France
[c] Centre des Matériaux, Mines Paris-Tech, 91000 Evry, France
[d] Institut PPRIME, UMR CNRS CNRS-ENSMA-Université de Poitiers, 86961 Futuroscope, France

A B S T R A C T

Titanium Matrix Composites (TMC's) containing various volume fractions of (TiB+TiC) particles have been deposited from powder feedstocks consisting of a blend of pre-alloyed (Ti-6Al-4V+B_4C) powders, using the direct metal deposition (DMD) laser process and the in-situ chemical reaction $5Ti+B_4C \rightarrow 4TiB+TiC$. Process optimization has allowed to obtain a homogeneous distribution of tiny TiB whiskers within the Ti-6Al-4V α/β matrix, with a full solubilization of C for low B_4C contents (0.5 wt% and 1.5 wt%), and the formation of a small amount of globular TiC particles at higher B_4C content (3%). Comparisons with Ti-6Al-4V DMD walls revealed a substantial grain refinement on TMC's due to enhanced grain nucleation on TiB whiskers, even for low B_4C contents. Last, mechanical investigations indicated an increase of 10–15% of Vickers hardness, and a constant 10% increase of Young modulus on a large temperature range (20–600 °C) for all B_4C content.

Keywords:
DMD
Laser
Titanium
Composites
TiB

1. Introduction

Titanium matrix composites strengthened with discontinuous ceramic particles appear to be attractive candidates to extend the use of titanium alloys up to 500 °C temperature in aeronautical parts. Such attractive properties are expected to come from high specific elastic moduli and strengths on a large range of temperatures, provided by homogeneous distribution of fine particles or whiskers. Among the possible reinforcement for Ti matrix composites, TiB and TiC have been widely considered as the most promising, due to a good chemical affinity with titanium allowing their formation and sound interfaces, combined with a rather low cost and ease of supplying. The combined use of TiB and TiC reinforcements was also shown to provoke synergistic effects to increase further the mechanical resistance of composites [1].

The manufacturing of TMC reinforced by TiB and/or TiC particles or whiskers has already considered with conventional or vacuum-aided casting techniques [1–3] and with powder metallurgy [4,5]. However, new layer additive manufacturing techniques offers alternative ways for obtaining directly complex 3D shapes. Among these techniques, the selective laser melting (SLM) "powder bed" technique allows obtaining complex architectures in a rather long process time [6] whereas direct metal deposition (DMD) laser technique manufactures in a shorter time bulk materials from CAD file, through layer additions involving melting - solidification events of a projected powder stream [7–10]. This DMD technique, derived from laser cladding process, also allows obtaining functional TMC surfaces, as shown in [11–13] against wear. More precisely, during a DMD process, a laser irradiation creates a small melt pool on the surface of a substrate. A stream of metal powders is fed into this melt pool to form a thin layer of matter and raise the global volume. The next layer is then built on the previous one, resulting in a 3D part. Making complex 3D shapes needs a pre-slicing of the part in a CAD model. The DMD process, which can be considered as a micro-casting technique with small (a few mm) melt-pools, induces a fast thermal loading $T=f(t)$, resulting in high heating and cooling rates approaching 10^3 K/s [14] and fast solidification rates in the cm/s range. This makes it a near out-of-equilibrium process compared with conventional casting techniques.

Several authors have already considered the ability to manufacture titanium matrix composites with laser additive manufacturing process [2–8], they aim to obtain near-net-shapes with optimum mechanical characteristics (high Young modulus, high specific strength, increased resistance at elevated temperature). In most of the studies reported so far, the use of Ti-base ceramic

* Corresponding author.
E-mail address: sebastienpouzet@hotmail.fr (S. Pouzet).

http://dx.doi.org/10.1016/j.msea.2016.09.002

particles such as TiB or TiC was shown to be beneficial due the good chemical compatibility of particles with Ti matrix that promoted good matrix/particle wetting and sound interfaces. An interesting option to obtain (TiB+TiC) ceramic reinforcements is the use of a reactive synthesis, through the injection of B_4C reactant in a titanium melt-pool to obtain the in-situ formation of TiC+TiB in the Ti matrix [10]. This option, has already been investigated with conventional processing routes such as vacuum arc melting or investment casting [1,2]. It has not been fully addressed yet with direct metal deposition (DMD) laser technique except in [10,11]. Such investigations have shown that 3 wt% B_4C was a maximum limit to ensure sufficient plasticity to titanium composites, and that a 4:1 ratio between B and C atoms was a good compromise.

One of the main issues of laser-based additive manufacturing processes reported so far in previous publications appears to be the lack of homogeneity of particles distribution in the titanium matrix, the occurrence of no-melted particles, and the resulting limited plasticity of laser-induced TMC's. It was also shown that wear properties of TMC-based coatings could be further enhanced by a step by step increase of the (TiC+TiB) vol% [11] whereas mechanical resistance of 3D structures were mostly shown to decrease above 5% vol TiC, TiB or (TiC+TiB), with an overall loss of plasticity. Following these works, a coaxial DMD process was used in the current study to manufacture titanium matrix composites walls, starting from a pre-mixed powder blend of Ti-6Al-4V+B_4C with B_4C contents of 0.5 wt%, 1.5 wt% and 3 wt%, corresponding to the in-situ exothermal formation (Eq. (1)) of up to 13% volume fraction of TiB reinforcements. Intrinsic properties such as geometric parameters (layer height and width), surface finish, microstructures, hardness, and mechanical resistance at ambient or temperatures up to 600 °C were investigated for various process parameters.

$$5Ti + B_4C \longrightarrow 4TiB + TiC \quad (1)$$

2. Experimental procedure

2.1. Powder blends

Two different powders were used for DMD tests: a +25–45 μm mean particulates Ti-6Al-4V (TLS Technik) powder with a spherical shape, and a irregular B_4C powder with nearly the same particulates distribution. Prior to DMD experiments, the two powders were blended (Fig. 1) and homogenized by rotation during 24 h with a TURBULA® shaker mixer in order to homogenize the blend. The powder blend was then dehydrated during 24 h at 75 °C in a drying cell.

2.2. DMD conditions

Two distinct conditions were used for DMD experiments (Table 1):

– For the first trials, an Yb:YAG laser (HL10002) operating at 1.03 μm and delivering 400–600 W continuous power in an uniform "top-hat" beam distribution was used. The powder stream, quasi-Gaussian in shape, was experimentally determined and exhibited a 3 mm diameter, with no specific effect of the B_4C content on powder stream shape (cf Section 3.1). During the DMD process (Fig. 2), the substrate was moved relative to the laser head, by a computer-aided routine, controlling the scan speed V, the wall length L (62 mm) and the layer height Δz value between subsequent passes (0.4–1 mm). Using an argon flow rate of 10 L min^{-1} to carry the powder and make a local gas shielding, the O_2 rate near the titanium melt-pool and below the nozzle was measured by an O_2 probe, and was shown to be less than 800 ppm. The resulting walls were used for metallurgical and morphological analysis.
– In a second step, and considering similar geometries but higher wall heights (up to 80 mm), additional experiments were carried out in an OPTOMEC Lens 850R industrial machine with less than 100 ppm O_2 content in the whole chamber. The manufactured walls were used mainly for mechanical investigations.

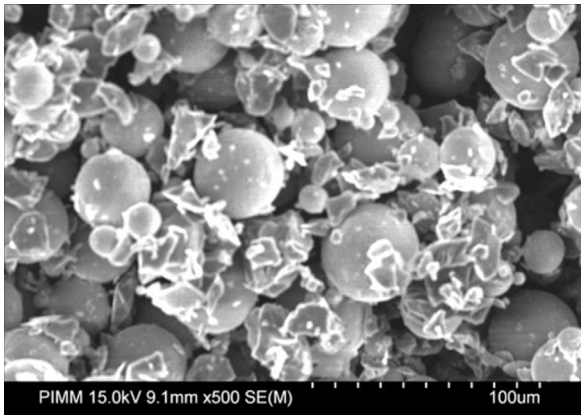

Fig. 1. SEM picture of a Ti-6Al-4V+3% B_4C powder blend before projection.

Table 1
Experimental DMD conditions (condition 1: with a local gas shielding=using an instrumented DMD set-up, condition 2: with a global gas shielding in the OPTOMEC Lens 850R DMD machine).

	P_0 (W)	V (mm/min)	D (mm)	Dm (g/min)	O_2 content (ppm)
1- Local shielding	400/600	200/400	1.7	2.5	≈2000
2- Global shielding	400/600	200/400	1.3	2.5	<100

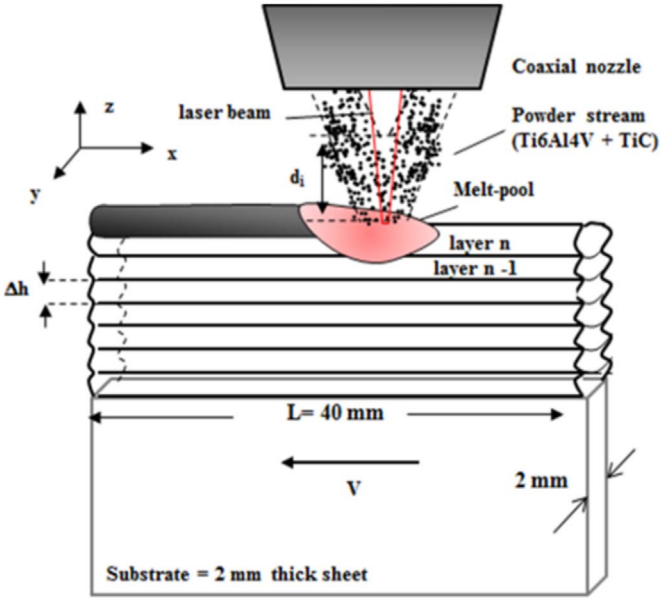

Fig. 2. Basic scheme of the Direct Metal Deposition laser process applied to the generation of Ti composites, starting from a thin titanium substrate.

For both cases, the following experimental conditions were used: (1) a 2 mm-thick Ti-6Al-4V substrate, a 15 s time pause t_p (s) between passes to homogenize thermal fields and layer growth,

(2) a constant mass feed rate D_m of 2.5 g min^{-1}, (3) a D = 1.7 mm laser spot diameter. In turn, the only variable parameters were the scanning speed V (0.2 m min^{-1} or 0.4 m min^{-1}) and the laser power P_0 (400 W or 600 W). For a 400 W laser power and a 0.2 m min^{-1} scan speed, the corresponding sample was called P400V200.

2.3. Geometrical, metallurgical and mechanical analysis of manufactured walls

The following features were analyzed on DMD walls:

– Dimensions and surface morphology of walls (roughness, waviness, and 3D profiles) was analyzed using a Veeco Dektak 150 profilometer in order to estimate a possible influence of C and B on melt-pool behavior (geometry, movement of the liquid metal) and resulting wall shapes.
– Microstructures were investigated on cross or longitudinal sections using both optical and scanning electron microscopy, after chemical etching with Kroll's reagent.
– Hardness distributions were measured on cross-sections, considering a 0.3 kg load, and automatic filiations directed in the −z direction of walls.
– Young modulus and mechanical resistance at ambient and elevated temperature were investigated using both the dynamic resonant method DRM (for the elasticity constant values E) [12],

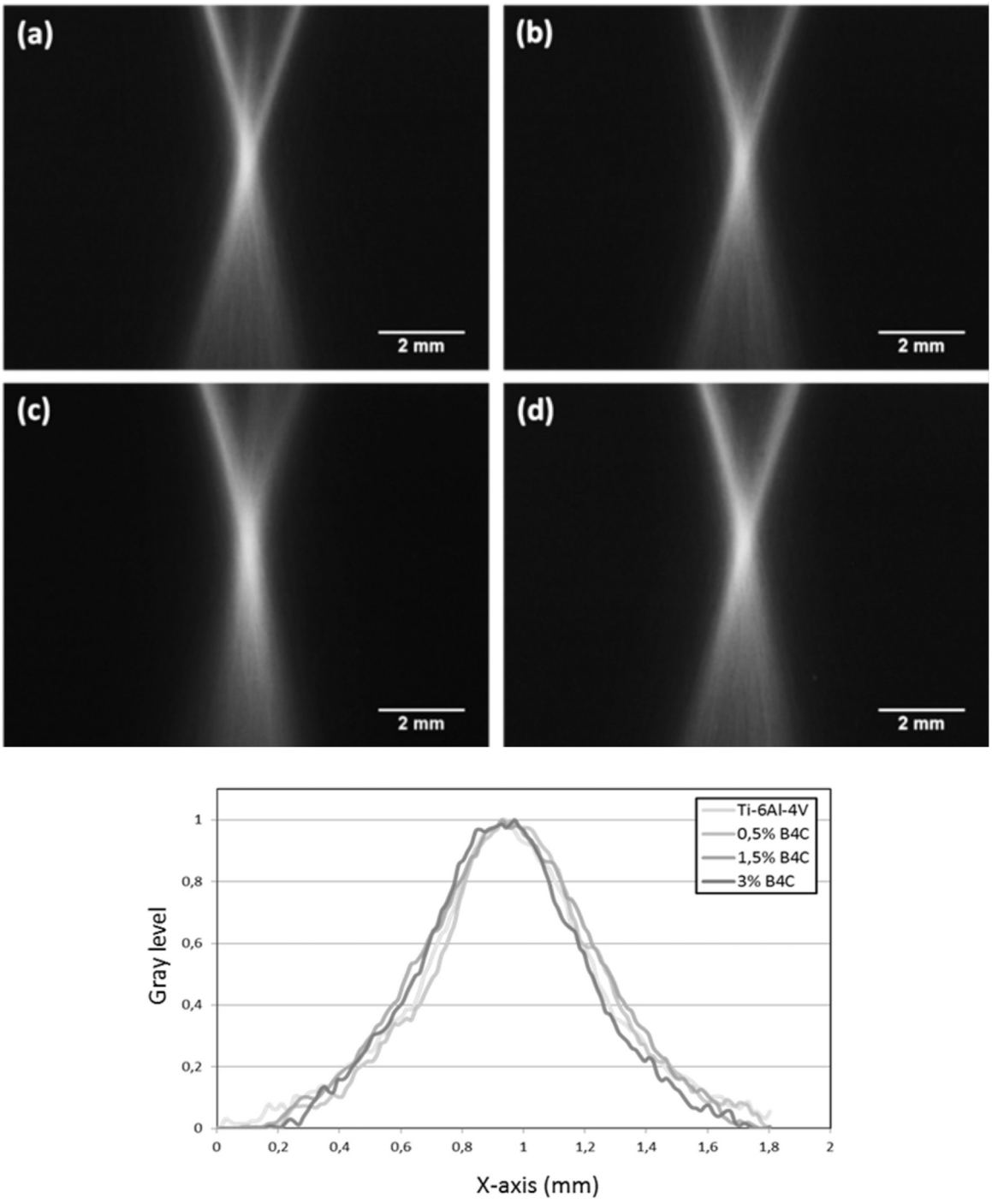

Fig. 3. Analysis of powder streams (a) 0% B_4C, (b) 0.5% B_4C, (c) 1.5% B_4C, (d) 3% B_4C.

and using tensile tests carried out under quasi-static loading conditions (10^{-3} s^{-1}) at 20 °C and 500 °C.

3. Experimental results

3.1. Analysis of powder streams

Powder streams, and their interaction with laser-induced melt-pools, are the main contributor to wall manufacturing in the DMD process. Consequently the analysis of powder streams, and especially those obtained with powder blends, is of a high importance to ensure a stable and efficient DMD process. Using a cold LED lateral illumination of the powder streams, and a CCD camera, the powder stream light diffusion was analyzed for both single Ti-6Al-4V powder and Ti-6Al-4V+B_4C pre-mixed powder. Then, using ImageJ software and a brightness level analysis, a 2D representation of powder streams was made possible. Such data indicated a low effect of B_4C addition on powder stream shape and diameter (Fig. 3), resulting in a widening of streams. Diameters of powder streams at half-maximum were shown to be equal to ≈ 1.2 mm.

3.2. Geometry of walls and surface finish

In the morphological analysis of walls, classical results are obtained, with: (1) an increase of layer heights Δh at low scan speeds ($\Delta h \approx 1$ mm for $V=0.2$ m min^{-1} and $\Delta h \approx 0.6$ mm for $V=0.4$ m min^{-1}) due to an increase of powder accumulation time $t_a = 2 \cdot r_{powder}/V$ (with r_{powder} = powder stream radius at focus position), (2) a widening of walls with increasing laser power, due an enlargement of fusion isotherms (Figs. 4 and 5).

Contrary to previous studies carried out on 8–15% TiC/Ti-6Al-4V composites [16], no clear modification of layer sizes (height, width) or roughness (Ra is near 20 μm) were shown with the addition up to 3% of B_4C. This seems indicate that:

- Boron did not play any tensio-active role in titanium melt-pools whereas carbon did,
- Thermo-physical properties of Ti-6Al-4V are not much affect by the precipitation of up to 15 vol% (TiC+TiB).

3.3. Microstructural analysis

Prior to microstructural analysis, cross sections at low magnification were analyzed for a constant B_4C rate (0.5%), and various process conditions. The grain orientation was shown to be mostly columnar for high powers (600 W: Fig. 6c and d), corresponding to higher manufacturing temperatures and dual (in-between oriented and equiaxial) for lower powers (400 W: Fig. 6a and b).

Microstructural analysis of walls revealed the formation of a dual microstructure composed of α/β Widmanstätten titanium matrix surrounding by TiB whiskers rather uniformly distributed as a network. The distribution of TiB whiskers was shown to be rather independent on B_4C mass ratio (Fig. 7). Above a given B_4C

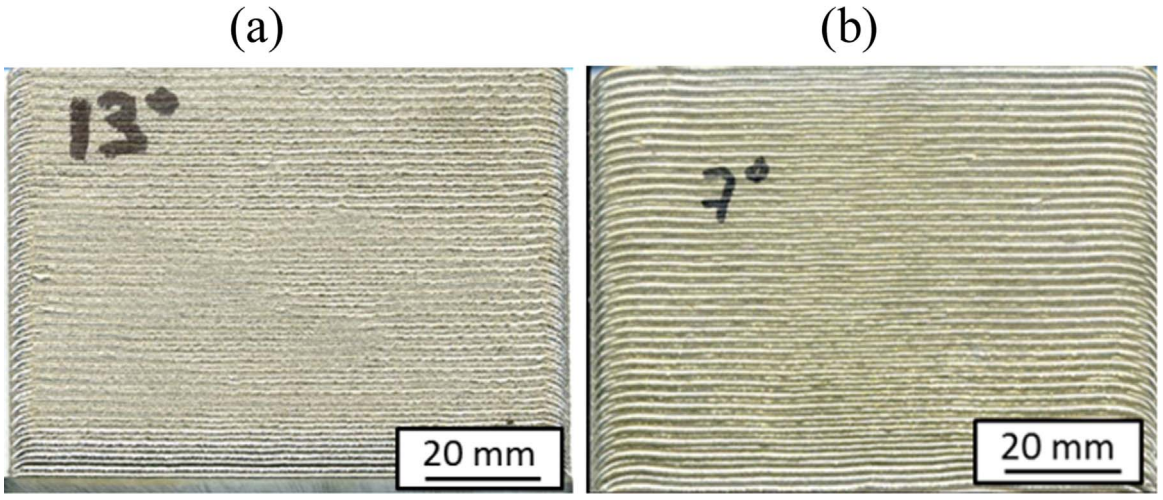

Fig. 4. Pictures of manufactured walls (1.5% B_4C) for a $V=200$ mm min^{-1} scanning speed: (a) P=400 W, (b) P=600 W.

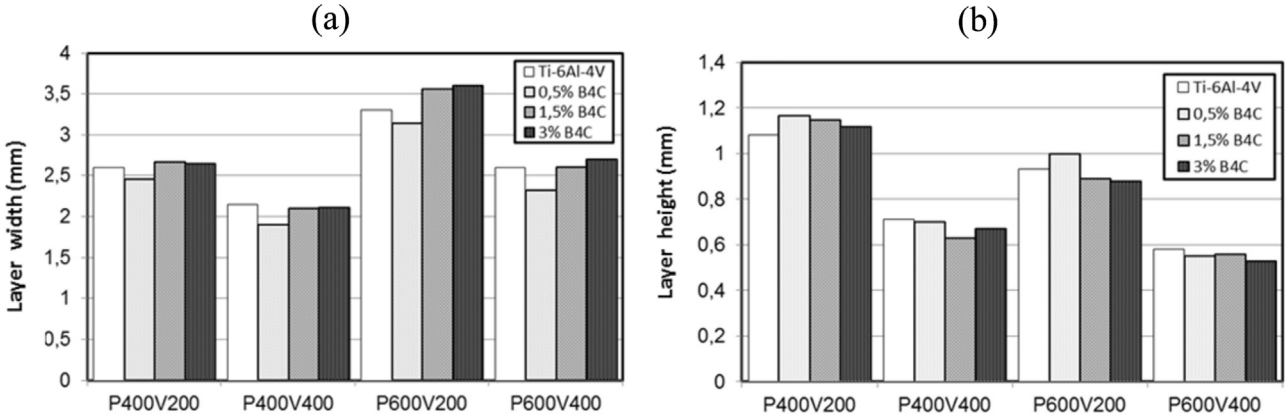

Fig. 5. Dimensions of manufactured walls versus % B_4C, (a) width, (b) layer height Δh.

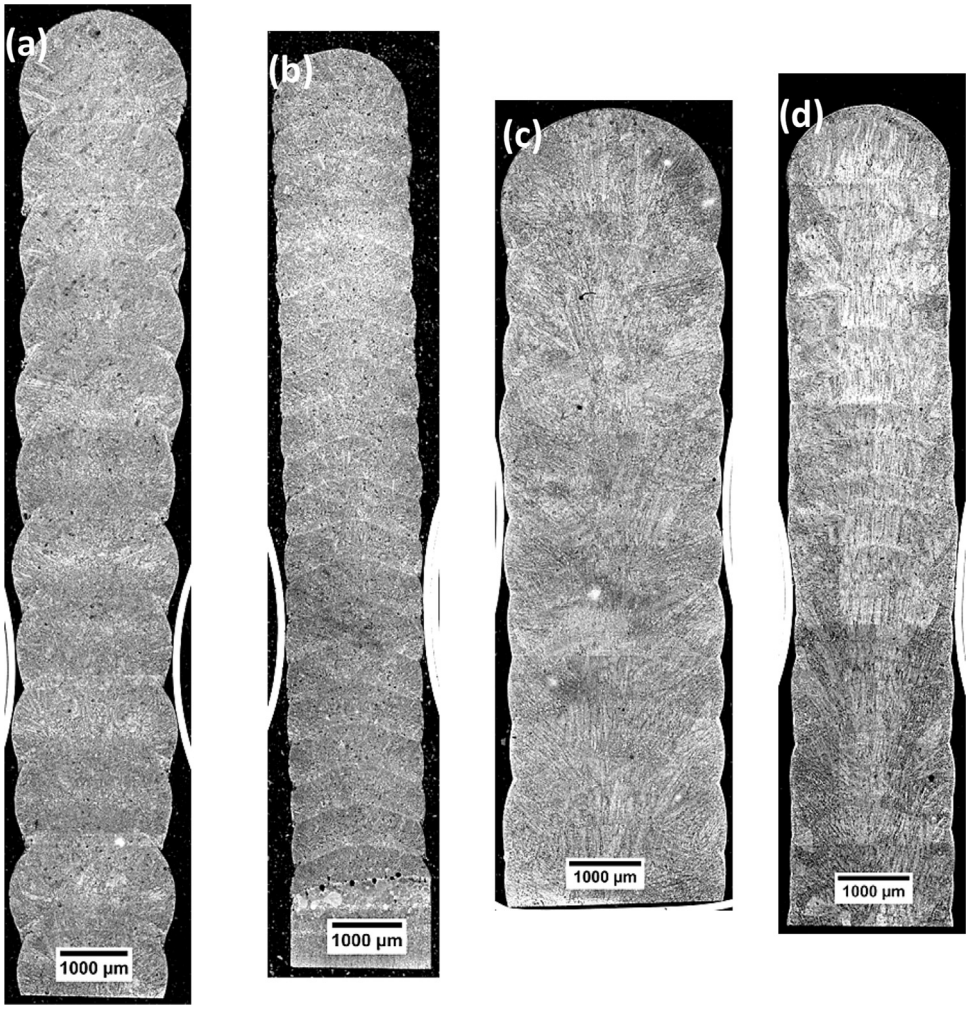

Fig. 6. Cross-sections of manufactured walls for 0.5% B_4C: (a) P400 V200, (b) P400 V400, (c) P600 V200, (d) P600 V400.

ratio (1.5%), TiB needles, and especially the shorter ones, seem to be mostly located at the position of former β-Ti grain boundaries. However, for higher ratios (3%), they also crystallize inside ex-β grains and exhibit longer shapes. At higher magnification (Figs. 8 and 9), two distinct TiB whiskers (95% short and 5% long) were identified and were attributed to different solidification modes (eutectic TiB for the shorter ones, and primary TiB for the longer). Their aspect ratio (L/l), which is known to be an important contributor to the reinforcement of titanium matrix composites [13] was shown to be between 10 (for 95% of short TiB needles) and 40 (for the remaining 5%), without any clear effect of B_4C content or process conditions.

For all the process conditions investigated so far, Ti matrix/TiB interfaces were sound due to the good chemical compatibility between Ti and TiB. Moreover, almost no porosities has be detected, except in the very first "cold" layers close to the substrate. For low powers (400 W), the number of non-melted B_4C particles was found to be slightly higher, but always inferior to 0.5% surface ratio.

It also has to be noticed that TiC particles, expected to be small and globular, were almost undetectable on DMD walls. Two possible reasons may explain this result: either TiC particles are too small (less than 0.5 µm) to be clearly detectable, or C atoms have been dissolved into a Ti-solid solution, with higher dissolubility than thermodynamically predicted [7], due to near-out of equilibrium conditions during rapid cooling ($Vc \approx 10^3\ K\ s^{-1}$). X-ray diffraction carried out on Ti-α allowed obtaining, through the evolution of a and c parameters of the hexagonal α-phase an estimation of solubilized carbon close to 0.5 at% which is four times higher than predicted by the Ti-C binary diagram. Above 1.5% B_4C, the evolution of a,c was shown to be less pronounced, indicating that the maximum solubility has been reached.

The oxygen concentration was measured within the walls for the two kind of gas shielding (local and global) (Table 2). As expected Oxygen is higher for the local shielding. The global gas shielding is used for the industrial machine, the oxygen concentration within the piece must be low to assure good mechanical property, the results obtained are consistent with the standards.

3.4. EBSD analysis of microstructures

The Electron BackScatter Diffraction (EBSD) technique was carried out in order to address grain size and crystal orientations in the matrix. Prior to EBSD analysis, the surface was polished with a sub-micron SiO_2 suspension in order to remove work-hardened layers due to the mechanical polishing, and improve the indexation. For the DMD condition investigated (P400V400), the indexation of former β-Ti grains revealed mostly equiaxial microstructures, with no preferential solidification axis (Fig. 10). It also highlight a severe grain refinement (Fig. 11: $D_{50} = 150$ µm on Ti-6Al-4V, 40 µm with 0.5% B_4C, 32 µm with 1.5% B_4C and 30 µm for 3% B_4C) and already discussed by previous authors like Sun et al. [2]. Such refinements with B_4C addition provide interesting

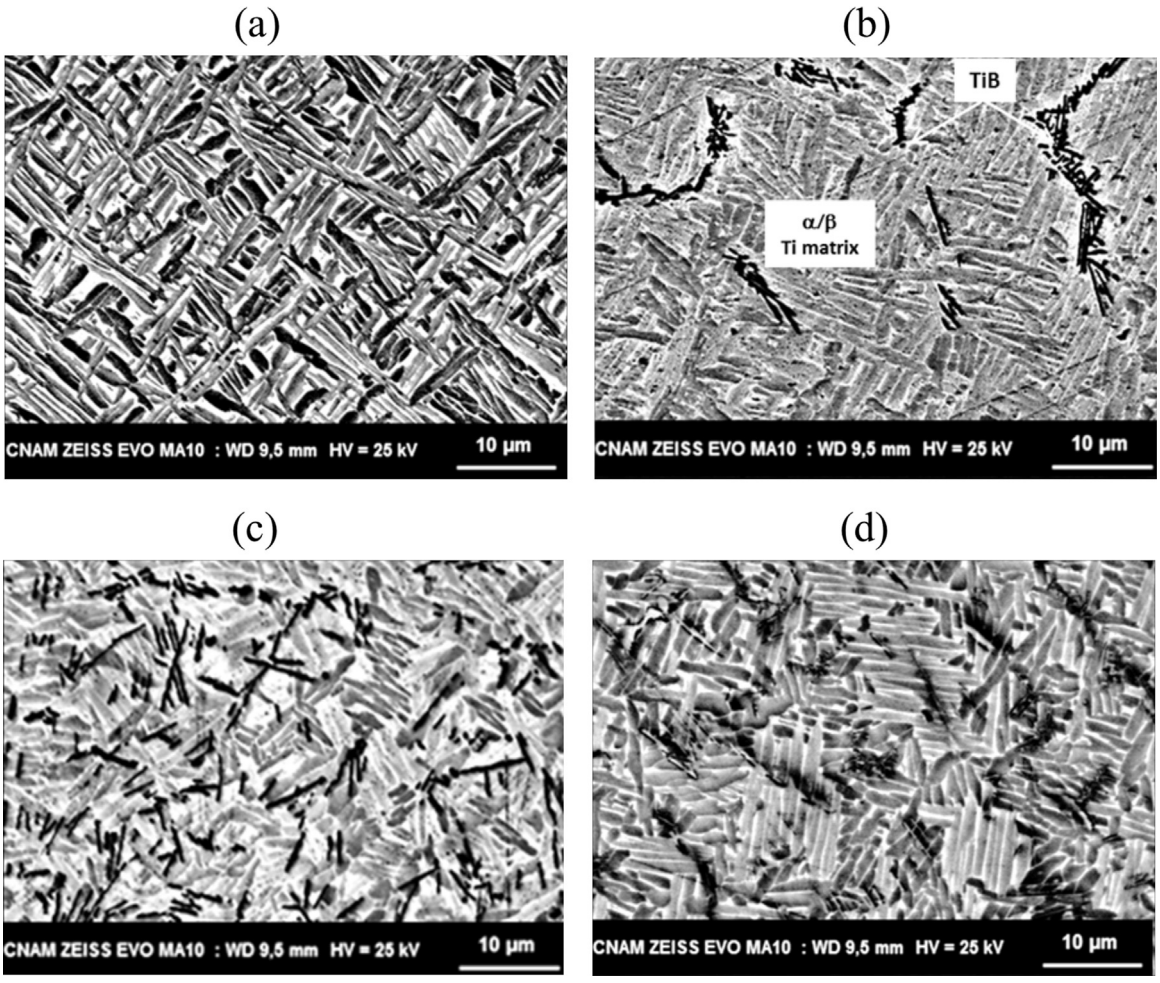

Fig. 7. SEM Microstructures of Ti-6Al-4V composites for (a) Ti-6Al-4V (b) 0.5% B_4C, (c) 1.5% B_4C, (d) 3% B_4C (P600V200).

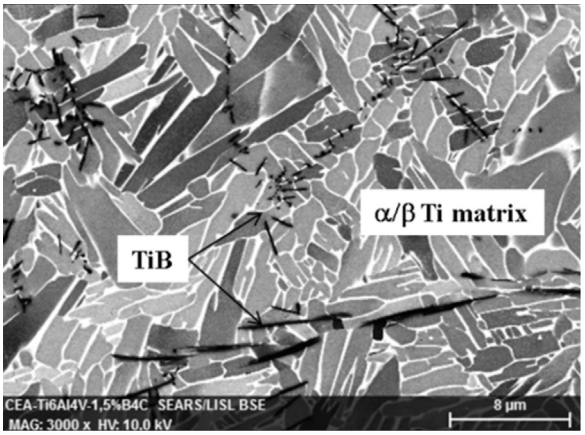

Fig. 8. SEM picture of a Ti-6Al-4V – 3% B_4C TMC.

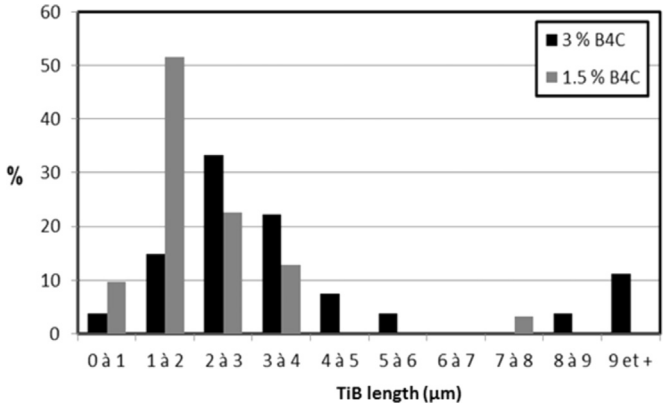

Fig. 9. Size distribution of TiB whiskers, occurrence of two distinct populations (1) near 95% short needles around 2 µm length, (2) 5% long needles around 8 µm length.

information about the solidification path of Ti-TiB composites that can be summarized as follows:

– Considering the Ti-B diagram, except for 3% B_4C, Titanium composites manufactured in this study can be considered as hypoeutectic, because B mass content is lower than 1.6%. Consequently, Ti-β is the first solid phase to occur during solidification,
– During Ti-β growth within the solidification range, boron is step-by-step rejected in the liquid and induces a micro-segregation of B towards β grain-boundaries until final eutectic solidification,
– At the eutectic temperature, small TiB whiskers precipitate on the precise location of β-grain boundaries and inhibit further grain growth.

Moreover, it is supposed that a macro-segregation of boron also occurred during solidification because of a variation of former β-Ti grain sizes along the z direction of the walls. This specific refinement (Fig. 10c) could be observed just below the top of each additive layer,

Table 2
analysis (vacuum remelting+gas phase chromatography) of O and N ratio for various B_4C contents and process parameters and for local (instrumented set-up) or global (industrial machine with Ar cell) gas shieldings. The difference of Nitrogen ratio between the two kind of gas shielding can not be explain, it could be due to a powder pollution.

Material	Parameters	shielding	Oxygen (%)	Nitrogen (%)
1.5% B4C	P600V200	Local Ar shielding	0.32	0.04
1.5% B4C	P600V200	Local He shielding	0.26	0.04
0.5% B4C	P400V200	Global Ar shielding (Optomec)	0.08	0.11
0.5% B4C	P600V400	Global Ar shielding (Optomec)	0.08	0.21

and was assumed to correspond to a non-remelted zone (no dilution). In this zone, a residual segregation of Boron towards the melt-pool surface occurred, followed by a non-fully remelt layer during the next layer, could enhance grain refinement effects.

On the other hand, large TiB needles, mostly shown at 3% B_4C, were assumed to be due to a hypereutectic primary germination and growth.

3.5. Mechanical investigations

3.5.1. Hardness tests

Vickers Hardness tests carried out with a 0.5 kg load show an average 95 HV hardness increase (360 $HV_{0.5}$ to 455 $HV_{0.5}$) due to

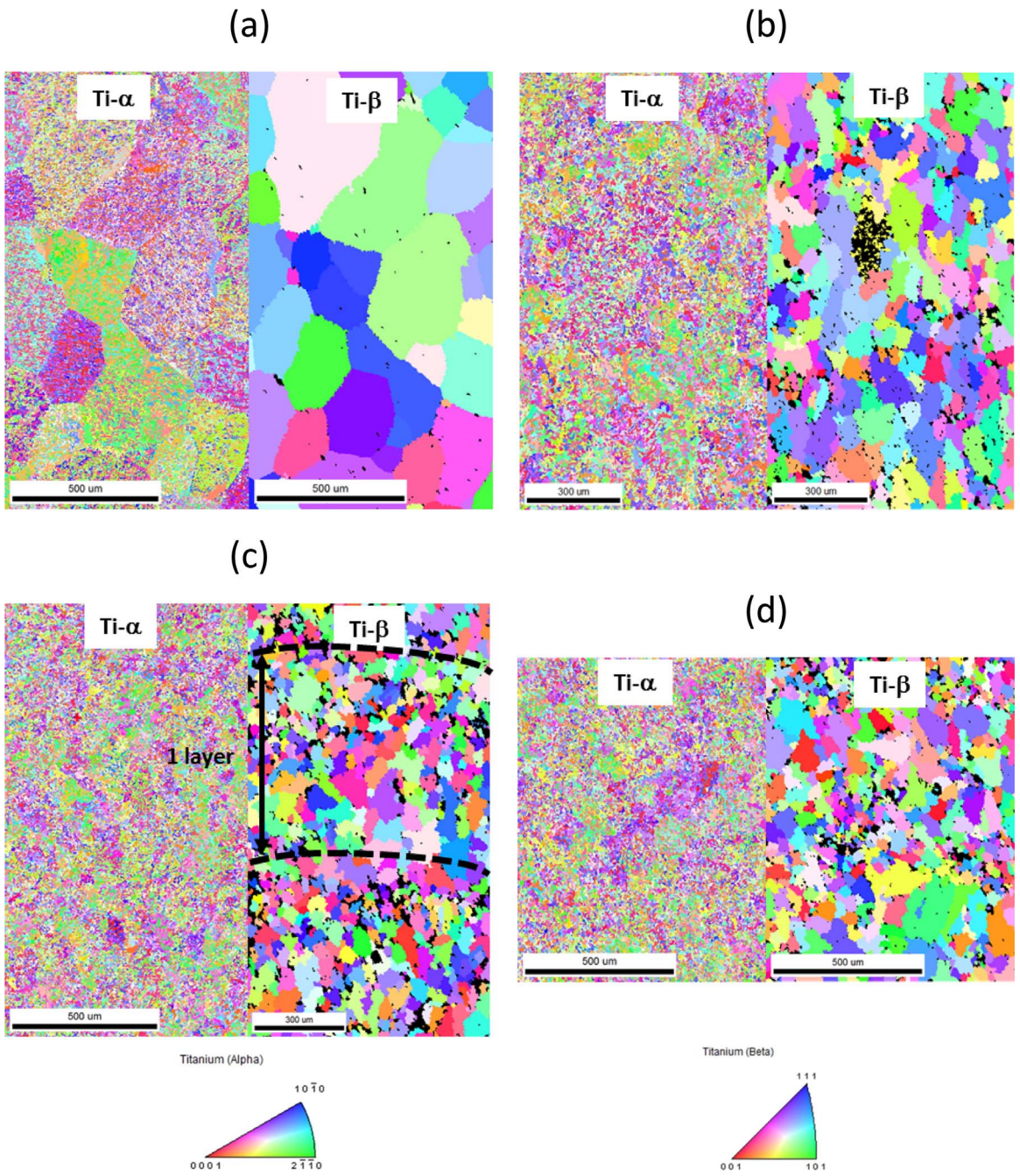

Fig. 10. EBSD analysis of Ti-6Al-4V α-Ti matrix and reconstruction of former β-grains for (a) 0% B_4C, (b) 0.5% B_4C, (c) 1.5% B_4C, (d) 3% B_4C (P400 V400) [17].

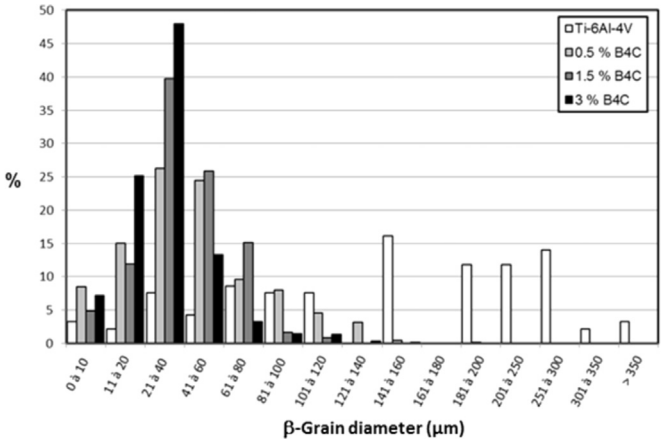

Fig. 11. Variation of former β-Ti grain size with B_4C ratio.

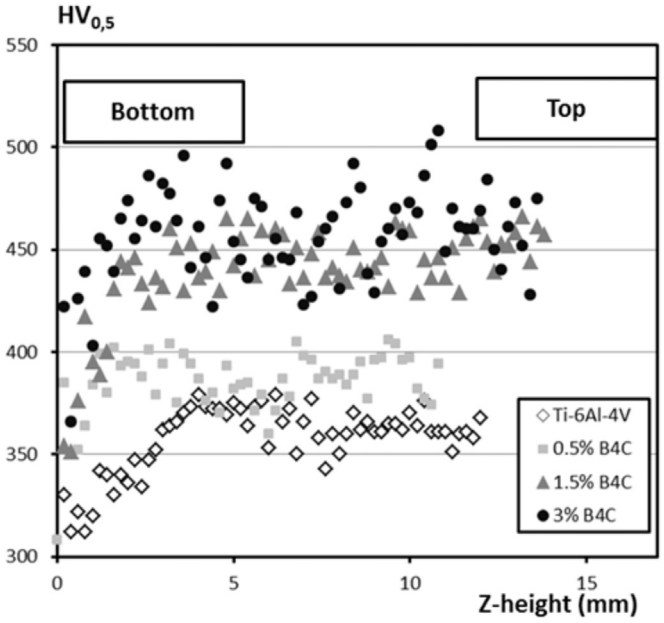

Fig. 12. Hardness measurements on DMD samples-Influence of the B_4C content.

the formation of up to 12 vol% TiB whiskers (Fig. 12), with higher dispersion on HV values for composites. A very small hardness gap was shown between 1.5% B_4C (6 vol% TiB = 445 $HV_{0.5}$), and 3% B_4C (12 vol% TiB = 455 $HV_{0.5}$). It was assumed the saturation of solubilized carbon (0.5 mass% C) above 1.5% B_4C, already mentioned in Section 3.2, created this hardness gap. This result also indicates that the carbon in solid-solution in α-Ti is the major contributor to the hardening of the composit e, and that further increases of TiB content above 1.5% B_4C did not play a dominant role on materials strengthening.

3.5.2. Measurement of elastic moduli

Young's longitudinal elastic moduli were investigated on a large range of temperatures (20–600 °C) using a dynamic resonant method in bending mode [12]. A constant +10 GPa increase of E values was evidenced on all the temperature range (Fig. 13), which confirms the potential benefit of using TiB reinforced Ti-6Al-4V matrix at high temperature. The reason why Young's modulus of 1.5% B_4C TMC becomes higher above 350 °C than the 3% B_4C TMC is not clear yet. A pronounced diffusion of carbon outside α-Ti matrix above 350 °C, could be a possible explanation. Another possibility

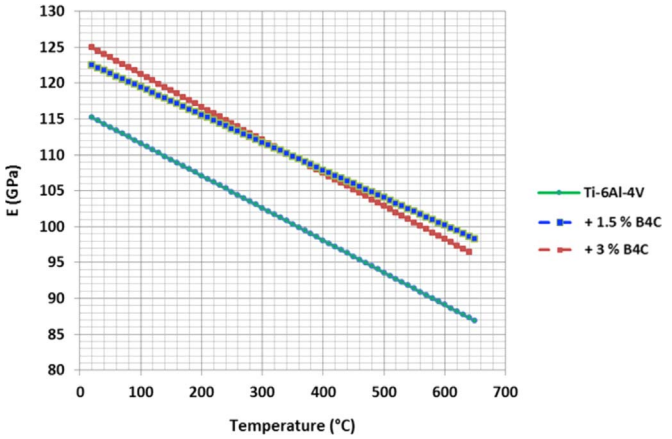

Fig. 13. Young's modulus determination using the Dynamic Resonant Method (P400V200 DMD condition).

could come from the TiB network around former β-Ti grains, which is kept nearly unchanged between 1.5% and 3% B_4C. This network could be the main reason why composite stiffness is increased, and it is constant (+10 GPa) with temperature. With such an explanation, one understands why Young's moduli are constant at 1.5 or 3% B_4C.

3.5.3. Tensile testing

Tensile tests were performed on Ti-6Al-4V and Ti-6Al-4V + 1.5% B_4C DMD specimens at ambient temperature and 500 °C, for different DMD conditions. Prior to tensile testing, samples were heat-treated at 600 °C during 2 h in order to get stress free sample.

Stress-strain curves (Fig. 15) obtained on Ti-6Al-4V indicate a major difference between L and T directions, whatever the process conditions. Samples machined along the longitudinal L direction (= direction of laser scanning), systematically exhibit better tensile behavior than transverse T samples machined along the layer growth (Fig. 14). At ambient temperature, the Ti-6Al-4V has a very low elongation (≈ 1%) in the T direction, and a correct ductility (around 4–5% elongation) in the L direction (Fig. 15a). Ultimate tensile strengths were shown to be close to 1000–1100 MPa. When the addition of 1.5% B_4C, the ductility tends to decrease and fracture occurs in the elastic regime, with UTS values between 1000 and 1200 MPa in the L direction, and around 700 MPa in the T direction (Fig. 15b).

At 500 °C, the composite has a better behavior than Ti-6Al-4V, with a 60 MPa increase of UTS (770 MPa → 830 MPa), and most of all, no difference between L and T directions (Fig. 15c and d). However, a decrease of elongation is also shown (9–6%), which traduces a loss of ductility on the composite. This loss of ductility was confirmed by SEM observations of fracture surfaces, where brittle inter-granular features are clearly shown on Ti-6Al-4V + 1.5% B_4C (Fig. 16b), compared with the classical ductile behavior of non-reinforced Ti-6Al-4V (Fig. 16a).

4. Discussion

Various aspects must be further discussed following our experimental work. Among these aspects:

- The carbon was assumed to play an extremely limiting role in the mechanical properties (plasticity) of the DMD composites.
- The in-situ formation of TiB needles was subject to opposite explanations in the literature.
- 1.5% B_4C and 3% B_4C have nearly the same microstructural and mechanical properties.

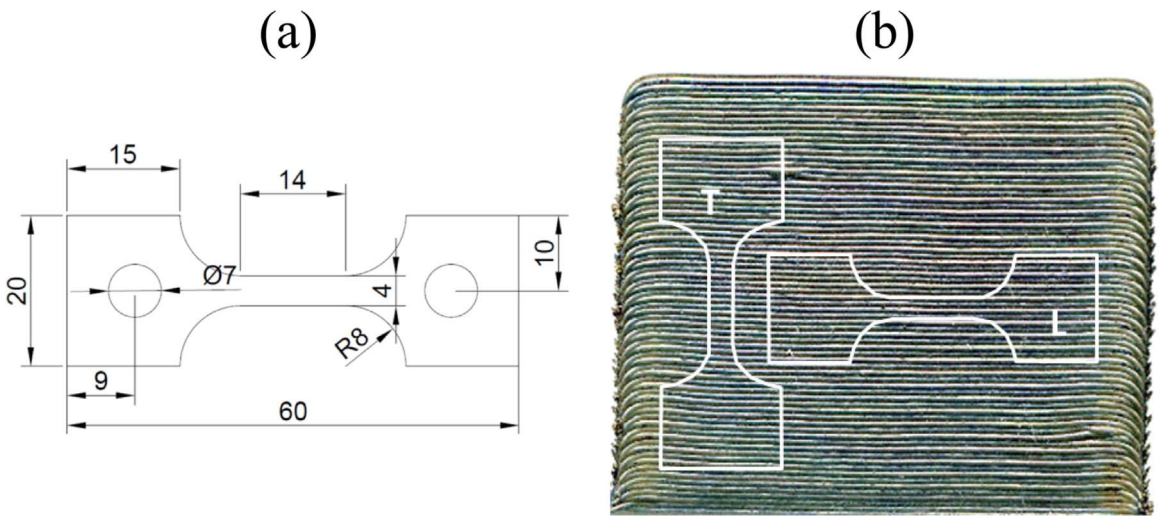

Fig. 14. (a) Tensile specimens, (b) L and T directions.

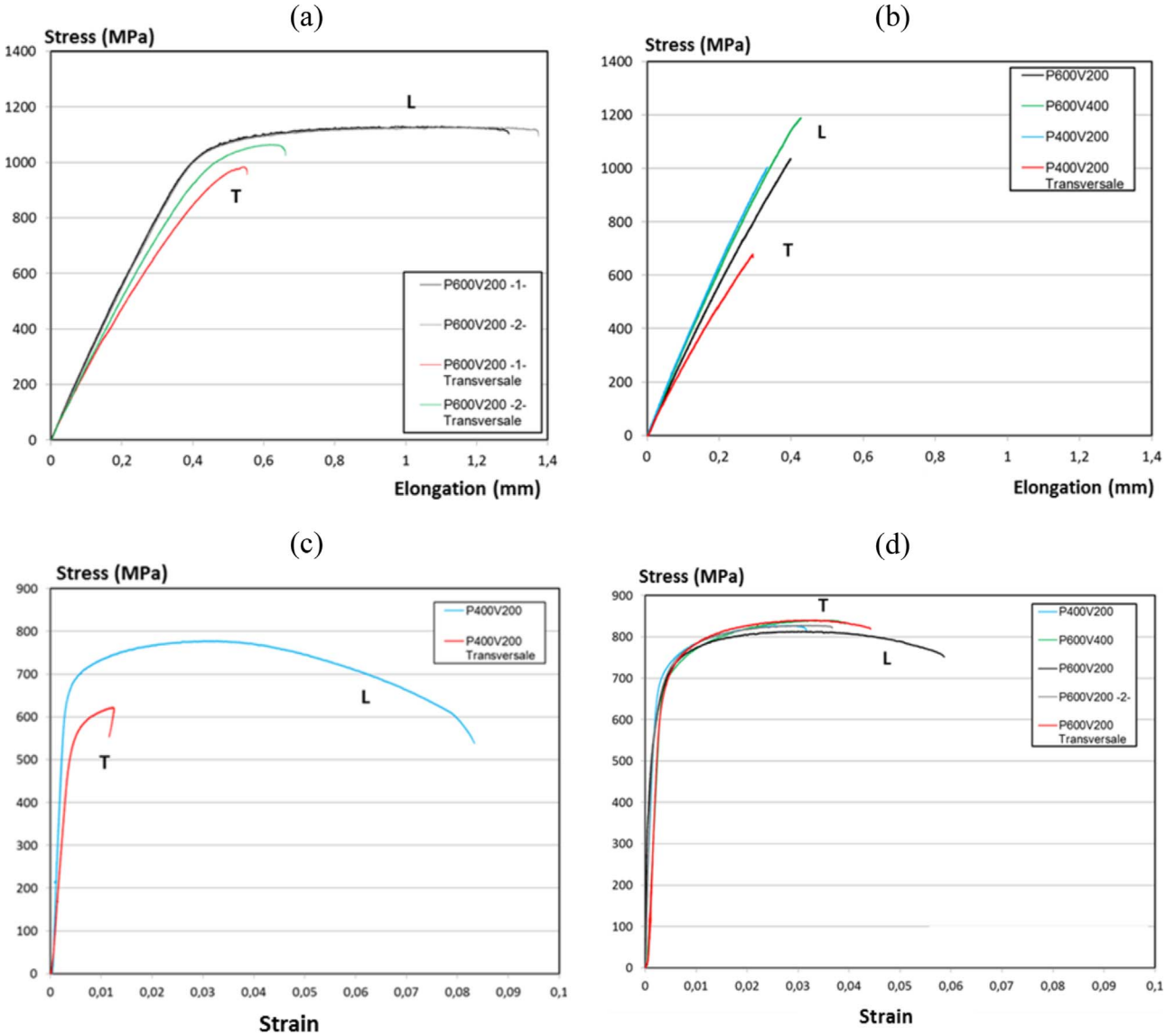

Fig. 15. Tensile tests on TMC for various process conditions: (a) Ti-6Al-4V at 20 °C, (b) Ti-6Al-4V + 1.5% B_4C at 20 °C, (c) Ti-6Al-4V at 500 °C, (b) Ti-6Al-4V + 1.5% B_4C at 500 °C.

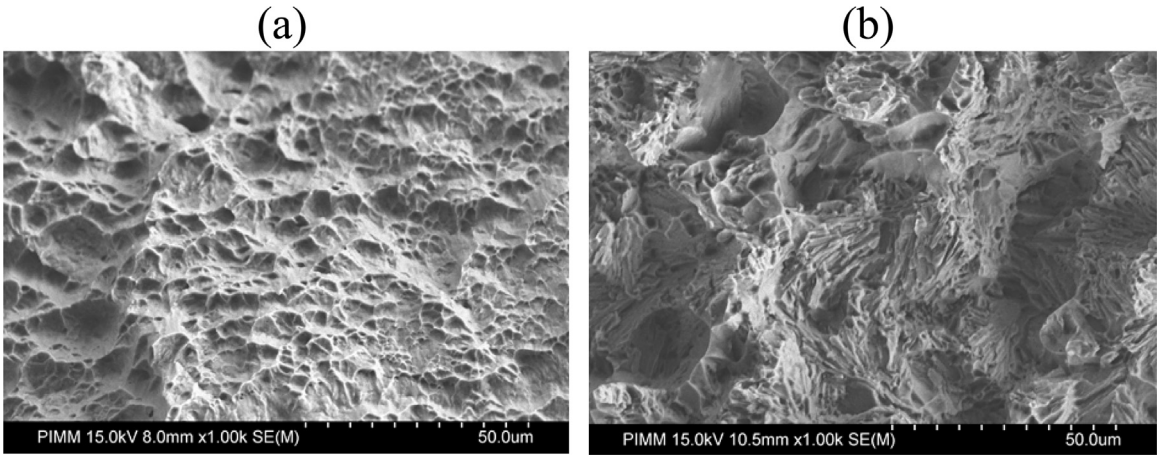

Fig. 16. SEM analysis of fracture at 500 °C: (a) Ti-6Al-4V, (b) Ti-6Al-4V + 1.5% B_4C.

First, considering the role of carbon, our microstructural investigations reveal a quasi-absence of TiC, which was attributed to a higher solubility of carbon in the α-Ti solid solution. This assumption is clearly justified by the high cooling rate involved in the DMD process. Numerical modeling carried by recent developments [15] indicate cooling rates varying between 200 and 700 K/s, that promote out-of-equilibrium solidification, and solubility thresholds higher than indicated by the binary Ti-C phase diagram (0.128 wt%). The same approach could have been used for boron. However, the boron solubility in α-Ti is close to 0, and the volume percent of TiB needles is very close to the calculation considering a full transformation of B in TiB.

We have proposed an original solidification path for our materials to explain the formation of small TiB needles around former β-Ti grains, and of large TiB needles within former β-Ti grains. Our explanation involves boron segregation during solidification, which provokes an enrichment of β-grains boundaries, just before precipitation of fine and eutectic TiB needles. The same explanation was proposed by Zhang et al. [10], whereas other authors had considered TiB needles as germination sites for β-Ti grains. An important point to notice is the specific microstructure of 3 wt% B_4C composites (=2.34 wt% B), which was expected to be mostly hyper-eutectic (with large primary TiB solidifying first), and which is finally very close to the microstructure of 1.5% B_4C samples (=hypoeutectic). To explain this artefact two assumptions are possible: (1) due to the high cooling rate, the Ti-B eutectic point (1.64 wt%) could be shifted towards larger B values, (2) the convection-aided chemical homogenization of the melt-pools was not sufficiently efficient to ensure an average hyper-eutectic composition on all the walls.

Rather similar properties (Young's moduli, Hardness) were obtained on 1.5% and 3% B_4C samples. On the one hand, if we consider that Young's moduli increases compared with Ti-6Al-4V can be mostly related to the TiB network (up to 12 vol%) around β-Ti grains, similar E values become rather logical. On the other hand, the constant hardness values for 1.5% and 3% B_4C samples can be clearly attributed to the saturation of C content in solid solution, which is the main contributor to matrix hardening. Tensile tests carried out on 3% B_4C should confirm this assumption.

Among the limitation of our study, one can mention the need of a precise measurement of carbon content in the α-Ti matrix (we only provide a rough estimation), for instance with microprobe analysis and a real estimation of β-Ti inter-lath residual phase, using higher sensitivity diffraction analysis (with our XRD set-up, crystallographic phase contents lower than 5% are hard to determine).

Oncoming analysis should be focused on lower B_4C contents (0.5% wt%) to limit the negative effect of carbon, and provide a good compromise between elongation and resistance during tensile tests.

5. Conclusion

Walls composed of titanium matrix composites (TMC) have been successfully fabricated with a blend of Ti-6Al-4V + B_4C powders, and using the direct metal deposition (DMD) laser process. Sound and homogeneous Ti-6Al-4V – TiB microstructures were globally obtained with a grain refinement attributed to boron segregation during β-Ti solidification. A specific zone was identified in the inter-layer areas which exhibited a small increase of TiB content, and a more pronounced grain refinement, without clear effect on the local hardness. The quasi-absence of TiC below 1.5% B_4C was attributed to an increase of C solubility in α-Ti at high solidification rate, which reduced the ductility of the composites at ambient and elevated temperatures. However, an increase of elastic moduli and UTS was demonstrated at elevated temperature (500 °C), which confirmed the potential of TMC versus non-reinforced titanium alloys.

Acknowledgments

Authors wish to thank N. Ranc from PIMM laboratory for his helpful on the tensile test, C. Blanc from CEA/DEN for helpful SEM analysis and C. Cayron from EPFL for the lending of ARPGE program.

References

[1] M.M. Wang, W.J. Lu, et al., Effect of volume fraction of reinforcement on room temperature tensile property of in-situ (TiB+TiC)/Ti matrix composites, Mater. Des. 27 (2006) 494–498.
[2] S. Sun, M. Wang, et al., The influences of trace TiB and TiC on microstructure refinement and mechanical properties of in-situ synthesized Ti matrix composites, Compos.: Part B 43 (2012) 3334–3337.
[3] J. Wang, et al., Microstructures and mechanical properties of investment casted titanium matrix composites with B_4C addition, Mater. Sci. Eng. A 628 (2015) 366–373.
[4] D.R. Ni, L. Geng, J. Zhang, Z.Z. Zheng, Effect of B4C particle size on microstructure of in-situ titanium matrix composites prepared by reactive processing of Ti-B4C system, Scr. Mater. 55 (2006) 429–432.
[5] M.Y. Koo, J.S. Park, et al., Effect of aspect ratios of in-situ formed TiB whiskers on the mechanical properties of TiBw/Ti-6Al-4V composites, Scr. Mater. 66 (2012) 487–490.

[6] T. Kühnle, K. Partes, In-situ formation of titanium boride and titanium carbide by selective laser melting, Phys. Procedia 39 (2012) 432–438.
[7] W. Liu, J.N. DuPont, Fabrication of functionally graded TiC/Ti composites by laser engineered net shaping, Scr. Mater. 48 (2003) 1337–1342.
[8] F. Wang, J. Mei, H. Jiang, X. Wu, Laser fabrication of Ti6Al4V/TiC composites using simultaneous powder and wire feed, Mater. Sci. Eng. A 445–446 (2007) 461–466.
[9] R. Banerjee, P.C. Collins, et al., Direct metal deposition of in-situ Ti-6Al-4V – TiB composites, Mater. Sci. Eng. A 358 (2003) 343–349.
[10] Y. Zhang, J. Sun, R. Vilar, Characterization of (TiB+TiC)/TC4 in-situ titanium matrix composites by laser direct deposition, J. Mater. Process. Technol. 211 (2011) 597–603.
[11] Y.S. Tian, C.Z. Chen, et al., Wear properties of alloyed layers produced by laser surface alloying of pure titanium with B4C and Ti mixed powders, J. Mater. Sci. 40 (2005) 4387–4390.
[12] P. Gadaud, Elastic properties characterization by means of the dynamic resonant technique, in: N. Ranganathan (Ed.), Materials Characterization – Modern Methods and Applications, Stanford Publisher, 2015 (Chapter 9).
[13] J. Liang, S. Chen, et al., Study on microstructure of laser in-situ formation of TiB_x and TiC titanium composite coatings, Mater. Sci. Forum 686 (2011) 646–653.
[14] J. Li, Z. Yu, Z.H. Wang, Microstructural characterization of titanium matrix composite coatings reinforced by in situ synthesized TiB+TiC fabricated on Ti6Al4V by laser cladding, Rare Met. 29 (5) (2010) 465–472.
[15] P. Peyre, R. Neveu, et al., Analytical and numerical modelling of the direct metal deposition laser process, J. Phys. D: Appl. Phys. 41 (2008) 025403.
[16] S. Pouzet, P. Peyre, C. Gorny, O. Castelnau, C. Colin, Direct metal deposition of titanium matrix composites: optimization of the process and microstructural analysis, in: Proceedings of International Congress on Applications of Lasers and Electro-Optics (ICALEO'2013), Orlando, USA, 2013.
[17] C. Cayron, ARPGE: a computer program to automatically reconstruct the parent grains from EBSD data, J. Appl. Crystallogr. 40 (2007) 1183–1188.